RSC Advances

PAPER

View Article Online
View Journal | View Issue

Cite this: *RSC Adv.*, 2025, **15**, 30046

Construction of magnesium–molybdenum–phosphorus multi-component flame retardant and its performance in flexible PVC composites

Xue Li,†[a] Xiaoyuan Liu, †[a] Zhihui Lv[abc] and Li Dang *[abc]

To address the high flammability and toxic smoke emission of flexible PVC (fPVC), a magnesium–molybdenum–phosphorus multi-component flame retardant (MO@MH-PEPE) was constructed by surface-modifying self-synthesized molybdenum oxide-hybridized magnesium hydroxide (MO@MH) with phenolic epoxy phosphate ester (PEPE). Fourier-transform infrared spectroscopy (FTIR), X-ray photoelectron spectroscopy (XPS), and scanning electron microscopy (SEM) confirmed the chemical grafting of PEPE onto MO@MH *via* P–O–Mg bonds, enhancing interfacial compatibility. When incorporated into fPVC, the fPVC/MO@MH-PEPE composite exhibited superior flame retardancy and smoke suppression: limiting oxygen index (LOI) increased to 32.0%, UL-94 reached V-0 rating, peak heat release rate (pHRR) and total smoke production (TSP) decreased by 47.16% and 75.15% compared with the fPVC/MH composite, respectively. The char residue yield (50.00 wt%) and graphitization degree significantly improved, attributed to Mo^{6+}/Mo^{4+} redox catalysis and phosphoric acid charring. Thermogravimetry analysis-FTIR (TGA-FTIR) revealed gas-phase flame inhibition *via* H_2O dilution. Furthermore, PEPE modification optimized mechanical properties, increasing tensile and impact strength by 28.35% and 6.50% over fPVC/MO@MH, supported by SEM-proven interfacial adhesion. This work demonstrates a synergistic Mg–Mo–P system for high-performance fPVC composites.

Received 18th June 2025
Accepted 16th August 2025

DOI: 10.1039/d5ra04341g

rsc.li/rsc-advances

1 Introduction

Polyvinyl chloride (PVC), one of the five major general-purpose plastics, exhibits excellent chemical resistance, processability, electrical insulation, and cost-effectiveness.[1] It is widely utilized in construction, packaging, electronics, medical equipment, and other industries. Based on its plasticizer content, PVC can be categorized into rigid, semi-rigid, and flexible types.[2] Flexible PVC (fPVC), due to the incorporation of over 40% plasticizers, demonstrates significantly increased flammability with a reduction in the limiting oxygen index (LOI) by approximately 24%.[3,4] More critically, during combustion, fPVC releases substantial amounts of toxic fumes, posing severe risks to human life and property, thereby restricting the application scope of fPVC products.[5,6]

Magnesium hydroxide (MH), as an environmentally friendly halogen-free flame retardant, offers advantages such as high heat absorption capacity, a high thermal decomposition temperature, and the ability to neutralize acidic gases generated during combustion.[7–9] However, MH relies mainly on physical insulation and dilution of combustible gases to exert its flame retardant effect. This has limitations in effectively suppressing material combustion and smoke emissions. In order to achieve the desired flame retardant effect, high amounts (often more than 50%) are usually required, which will seriously weaken the mechanical properties of the material.[10,11] In order to solve this problem, in recent years, researchers have begun to work on combining traditional flame retardants with transition metal oxides or salts to improve the flame retardant and smoke suppression efficiency of polymer materials by virtue of the catalytic carbonization or free radical scavenging ability of transition metal compounds.[12–15] For example, Cheng *et al.* constructed BiOCl@Cu-MOF hybrid materials on BiOCl surfaces using an *in situ* growth strategy and incorporated them into PVC coatings, effectively reducing peak smoke generation (pSPR) by 66.7%, total smoke emission (TSP) by 50.3%, and peak heat release rate (pHRR) by 55.9%.[16] Bi *et al.* constructed Fe-PDA modified layer (MDH@Fe-PDA) by loading polydopamine chelated iron ion on magnesium hydroxide (MDH) surface *in situ*, and introduced it into epoxy resin (EP) system cooperatively with MDH. The results showed that when the total flame retardant content was 30 wt%, the pHRR and pSPR of EP composite decreased by 57% and 67%, respectively.[17] These studies demonstrate that the synergistic flame retardant system

[a]*School of Chemical Engineering, Qinghai University, Xining 810016, China. E-mail: danglix@163.com*

[b]*Salt Lake Chemical Engineering Research Complex, Qinghai University, Xining 810016, China*

[c]*Key Laboratory of Salt Lake Chemical Material of Qinghai Province, Qinghai University, Xining 810016, China*

† These authors contributed equally to this work: Xue Li, Xiaoyuan Liu.

containing transition metal components has significant advantages in improving flame retardancy and smoke suppression.

Based on this, nano molybdenum oxide (MoO_3), as a transition metal oxide with strong Lewis acidity and redox activity, has excellent catalytic carbonization ability, and shows promising applications in flame retardancy.[18–20] In our prior research, MoO_3 hybrid MH (MO@MH) was successfully prepared by one-step hydrothermal method.[21] The findings indicated that MO@MH substantially improved the flame retardancy and smoke suppression properties of fPVC composites. The quality, density and integrity of the char residue of fPVC/MO@MH composites were significantly improved compared with that of fPVC/MH composite. The +6 Mo element participated in the charring process of fPVC matrix through oxidation–reduction reactions to form +4 Mo compounds.[22] MO@MH still faces critical challenges: MO@MH has poor compatibility with polymer matrix and is easy to agglomerate, thus affecting its uniform distribution in the matrix. This issue is commonly observed in various inorganic/polymer composite fields. Researchers typically employ surface modification techniques to treat inorganic fillers, introducing organic functional groups onto their surfaces to enhance interface compatibility[23,24] and bonding strength with polymer matrices such as fPVC. Simultaneously introducing phosphorus,[25] silicon,[26] nitrogen,[27] or other flame-retardant elements (or groups) is expected to improve flame retardant efficiency while addressing mechanical property concerns.[28,29] Notably, phosphorus-containing modifiers, due to their synergistic effects, can simultaneously enhance interface compatibility and further augment flame retardancy. In our previous work, two different phosphorus-containing modifiers, epoxy phosphate ester (EPE)[30] and phenolic epoxy phosphate ester (PEPE),[31] were synthesized successfully and performed well in enhancing flame retardancy and smoke suppression properties of fPVC/MH composite. In comparison, PEPE performed better than EPE since the higher phosphorus content.

To address the aforementioned challenges, this study employed PEPE as the modifier for the surface modification of MO@MH, constructing a magnesium–molybdenum–phosphorus multi-component flame retardant. The impacts of these multi-component flame retardants on the flame retardancy, smoke suppression and mechanical properties of fPVC composites were systematically investigated. Modification effects were characterized using Fourier-transform infrared spectroscopy (FTIR), X-ray photoelectron spectroscopy (XPS), and scanning electron microscopy (SEM). Thermal stability was assessed by thermogravimetric testing (TGA). Flame retardancy and smoke suppression properties were evaluated *via* limiting oxygen index (LOI), vertical combustion (UL 94) and cone calorimeter tests (CCT). The char residues were observed and analyze by scanning electron microscopy (SEM), energy dispersive spectrum (EDS), Raman spectroscopy, X-ray photoelectron spectroscopy (XPS), *etc.* The gas phase flame-retardant and smoke-suppression mechanism was explored using thermogravimetry analysis (TGA)-FTIR. Mechanical behavior was analyzed through tensile and impact testing. This study aims to develop a flame retardant with superior flame retardancy, smoke suppression and mechanical properties using PEPE modification, providing novel insights and theoretical guidance for the advancement of PVC flame retardants. Furthermore, the findings hold significant reference value for the flame retardant modification of other polymers.

2 Experimental

2.1 Material

Low-viscosity phenolic epoxy resin (SNE-625, AR grade, Hunan Serwei New Material Technology Co., Ltd), orthophthalic acid (GR grade, Titan Technology Co., Ltd), acetone (AR grade, Sichuan Xilong Science & Technology Co., Ltd), polyvinyl chloride (SG-5, industrial grade, Inner Mongolia Juncheng Chemical Industry Co., Ltd), dioctyl phthalate (DOP, 95%, AR grade, Shanghai Maclin Biochemical Technology Co., Ltd), PVC processing additives (ACR-401, industrial grade, Qingdao Best New Material Technology Co., Ltd), glycerol monostearate ($C_{21}H_{42}O_4$, ≥90%, AR grade, Shanghai Maclin Biochemical Technology Co., Ltd), organotin heat stabilizer ($C_{22}H_{44}O_4S_2Sn$, Sn > 18,8%, AR grade, Shanghai Maclin Biochemical Technology Co., Ltd), liquid paraffin wax (AR grade, Tianjin Hedong District Red Rock Reagent Factory), magnesium hydroxide ($Mg(OH)_2$, AR grade, Tianjin Damao Chemical Reagent Factory), ammonium heptamolybdate ($(NH_4)_6Mo_7O_{24}\cdot 4H_2O$, AR grade, Tianjin Oubokai Chemical Co., Ltd), and sodium hydroxide (NaOH, AR grade, Tianjin Yongda Chemical Reagent Co., Ltd) were used in this study.

2.2 Preparation of PEPE and MO@MH

The preparation methods of PEPE and MO@MH both refer to our previous reports. Dissolve 10.00 g of EPN in 30 mL of acetone and stir magnetically at room temperature until EPN is completely dissolved. Subsequently, 4.65 g of orthophosphoric acid was mixed with 10 mL of acetone and added dropwise to the 65 °C EPN solution *via* a dropping funnel at a rate of approximately 1 drop/s. After completion of the dropwise addition, magnetic stirring (30 rpm) was maintained for 4 h, followed by dropwise addition of 30 mL of deionized water, and the reaction was continued for 1 h. At the end of the reaction, acetone was removed at 60 °C using a rotary evaporator to obtain crude PEPE as a yellow emulsion. The crude product was extracted by chloroform/water (volume ratio 1 : 2) system, the oil phase was separated and chloroform was removed by vacuum distillation, finally a white emulsion PEPE product was obtained.[31]

Ammonium heptamolybdate was dissolved in deionized water to prepare 0.035 mol L^{-1} ammonium molybdate solution; magnesium hydroxide was added according to Mg : Mo molar ratio of 1 : 1, and mixed and reacted for 10 min under stirring conditions to obtain a uniform slurry. The slurry was then transferred to a PTFE lined autoclave (filling degree not exceeding 60%) and subjected to hydrothermal reaction at 160 °C for 10 h under a stirring rate of 5 Hz. After the reaction, the white suspension obtained is filtered, washed with deionized

water, and dried at 80 °C for more than 6 h to finally obtain the nano molybdenum oxide hybrid magnesium hydroxide composite material (MO@MH).[21] The chemical structure of PEPE and XRD pattern of MO@MH were presented in Fig. S1 and S2, respectively.

2.3 Preparation of PEPE functionalized MO@MH

PEPE functionalized MO@MH (MO@MH-PEPE) was prepared *via* a wet modification process: 10.00 g MO@MH was added into 200 mL of deionized water with magnetic stirring for 10 min in order to obtain a pre-dispersed slurry of MO@MH. Then a certain amount of PEPE (mass ratio of MO@MH to PEPE = 100 : 5) was added into the pre-dispersed slurry of MO@MH which had been heated to 65 °C. The modification reaction was continued under magnetic stirring at 30 rpm for 1 h. The product was cooled to room temperate, then filtered and washed with plenty of ethanol and deionized water successively to remove excessive PEPE. Finally, the magnesium–molybdenum–phosphorus multi-component flame retardant was collected and dried at 60 °C for 12 h.

2.4 Preparation of fPVC composites

PVC powder, ACR-401, glycerol monostearate, DOP, liquid paraffin, organic tin heat stabilizer and MH(MO@MH, or MH@MO-PEPE) were added to the mixer according to the mass ratio of 100 : 4 : 0.6 : 40 : 0.4 : 2 : 20, and the pre-mixture was mixed in a two-roll open mill at 145 °C. The mixing time was 12 min, and the fPVC composite was obtained. The obtained fPVC composite material was placed in the plate vulcanization press to make a certain thickness of the sheet, the sheet temperature was 150 °C, the low pressure, high pressure and cooling time were 6 min; the composite sheet was cut into dumbbell type, straight type (notched and notched) splines by an electric punching machine to carry out various performance tests. The naming and formulation of the composite materials are shown in Table 1.

2.5 Characterization

Fourier transformation infrared spectra (FTIR) were investigated in Bruker INVENIOS fourier transform infrared spectrometer (Bruker, Germany) over 4000–400 cm^{-1} with resolution of 4 cm^{-1}.

The morphologies of MO@MH, MO@MH-PEPE, cross section of fPVC composites and char residues after cone calorimeter tests were all examined using a Merlin Compact scanning electron microscope (SEM, Zeiss, Germany) equipped with an energy-dispersive X-ray spectrometer (EDS).

XRD patterns were determined by a X'Pert X-ray spectrometer (Philips, Nederland) using Cu Kα radiation with a tube voltage of 40 kV and a tube current of 35 mA.

XPS was carried out using an ESCALAB Xi^+ multifunction electron spectrometer (Thermo Scientific, USA) equipped with an Al Kα X-ray source. The survey XPS spectra were taken in the constant analyzer energy mode with a pass energy of 100 eV and an energy step size of 0.4 eV, and high-resolution XPS spectra of C 1s, O 1s, P 2p and Mo 3d were also recorded with an energy step size of 0.125 eV.

The particle size distribution of MO@MH and MO@MH-PEPE was measured by a laser particle size analyzer (Malvern Laser Particle Size Analyzer 3000).

Thermogravimetry analysis (TGA)-FTIR was performed by a STA449F3 TG (Netzsch, Germany) coupled with a INVENIOS FTIR (Bruker, Germany). The temperature was raised from 30 to 800 °C at a heating rate of 10 °C min^{-1}. The flow rate of the carrier gas (high-purity N_2) was 70 mL min^{-1}. The temperature of the transfer line between TG and FTIR apparatuses was 230 °C. The resolution and range of FTIR were 4 cm^{-1} and 4000–600 cm^{-1}, and the spectrum was recorded per 21 seconds.

Limiting oxygen index (LOI) was carried out in a JP-6 oxygen index meter (Nanjing Shine Ray Instruments and Equipments Co. Ltd, China) with samples of 80 × 10 × 4.0 mm^3, following the procedure described in the ASTM D2863 standard.

According to ISO 5658-2, the vertical combustion grade was tested by HK-HVR horizontal and vertical testing machine (Zhuhai Huake Instruments and Equipment Co. Ltd, China), and the sample size was 125 × 10 × 1.5 mm^3.

Cone calorimeter tests were performed with samples of 100 × 100 × 3.0 mm^3 on a CCT cone calorimeter (Kunshan Motis Combustion Technology Instrument Co., Ltd, China) on the basis of standard ISO 5660-1. All samples were wrapped by an aluminum foil layer and then horizontally irradiated at a heat flux of 35 kW m^{-2}.

TGA was carried out using a STA449F3 thermal analyzer (Netzsch, Germany) at a heating rate of 10 °C min^{-1} under nitrogen atmosphere.

The Raman spectra of char residues were recorded by a LabRAM HR Evolution Laser Raman spectrometer (HORIBA Jobin Yvon Co. Ltd, France) with excitation provided in back-scattering geometry by a 514.5 nm argon ion laser.

Tensile strength was measured at room temperature with an ETM-B Electronic universal testing machine (Wance Group,

Table 1 Formulations of fPVC composites[a]

Sample	PVC (phr)	MH (phr)	MO@MH (phr)	MO@MH-PEPE (phr)
fPVC	100	—	—	—
fPVC/MH	100	20	—	—
fPVC/MO@MH	100	—	20	—
fPVC/MO@MH-PEPE	100	—	—	20

[a] All samples shown in Table 1 also contain DOP (40 phr), GMS (0.6 phr), ACR (4 phr), organic tin (2 phr) and paraffin wax stabilizer (0.4 phr), except for PVC (100phr) and the flame retardants (20 phr).

China) according to ISO 527-2: 1993 at 10 mm min^{-1} using dumbbell-shaped specimens of 750 mm in length and 2 mm in thickness.

The unnotched Izod impact strengths was measured using a 501J-4 plastic impact tester (Wance Group, China) according to ASTM D256-10 with the sample size was 80 × 10 × 4 mm^3.

3 Results and discussion

3.1 Characterization of MO@MH-PEPE

The chemical composition of magnesium–molybdenum–phosphorus multi-component flame retardant, MO@MH-PEPE, was systematically characterized using FTIR spectroscopy, as illustrated in Fig. 1. In the PEPE spectrum, the medium-intensity absorption band at 3369 cm^{-1} corresponds to the O–H stretching vibration, with peak broadening resulting from hydrogen bonding interactions. A weak band observed at 2398 cm^{-1} is assigned to the P–O–H stretching vibration, while the characteristic bending vibrations of aromatic C=C bonds in the benzene group manifest as two weak absorption features at 1510 and 1455 cm^{-1}. The strong absorption at 1236 cm^{-1} originates from P=O stretching vibrations, and the medium-intensity peak at 998 cm^{-1} is characteristic of P–O–C groups. In the MO@MH-PEPE spectrum, a weak band at 3645 cm^{-1} associated with free O–H stretching vibrations and a water adsorption-related bending vibration at 1650 cm^{-1}, both consistent with the MO@MH. More importantly, three spectral changes confirm the chemical modification: (1) a blue-shifted P=O vibration appears at 1244 cm^{-1} (pink inset), (2) complete disappearance of the P–O–H characteristic band at 2398 cm^{-1} (yellow inset), and (3) a significant 64 cm^{-1} blue shift of the P–O–C vibration to 1062 cm^{-1} (gray inset), indicative of P–O–Mg bond formation.[32] These observations collectively suggest that PEPE binds to the surface of MO@MH through a reaction between P–O–H and Mg–O–H groups, forming stable P–O–Mg covalent linkages.

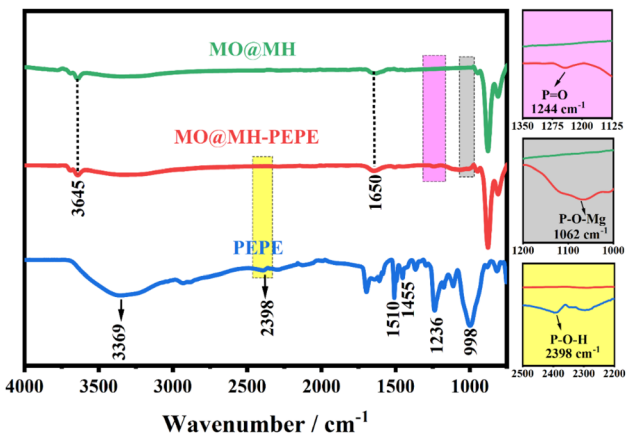

Fig. 1 FTIR spectra of MO@MH, MO@MH-PEPE, and PEPE.

SEM images of MO@MH and MO@MH-PEPE are presented in Fig. S3 and 2. As shown in Fig. S3(a) and (b), MO@MH is a flaky stacked flower spheroid structure with an overall size of 20–30 μm and a thickness of 10–20 nm. Compared with MO@MH, MO@MH-PEPE is irregularly stacked with clusters of flowers. High-magnification imaging (Fig. S3(d)) shows substantial surface modifications characterized by adherent particles and folded textures (yellow arrows), suggesting that PEPE incorporation induces microstructural alterations through either chemical modification or physical adsorption. To verify this viewpoint, the element composition of MO@MH-PEPE is characterized by EDS spectrum and elemental mappings. As shown in Fig. 2(b)–(f), the elemental distribution aligns essentially with the sample profile, especially for the uniform presence of P element throughout the structure, conclusively demonstrates the successful surface coating of MO@MH with PEPE modifier. The atomic fractions of Mg, O, Mo, P and C elements are 18.85 at%, 53.96 at%, 8.48 at%, 1.79 at% and 16.92 at%, respectively. Compared with MHPEPE (a

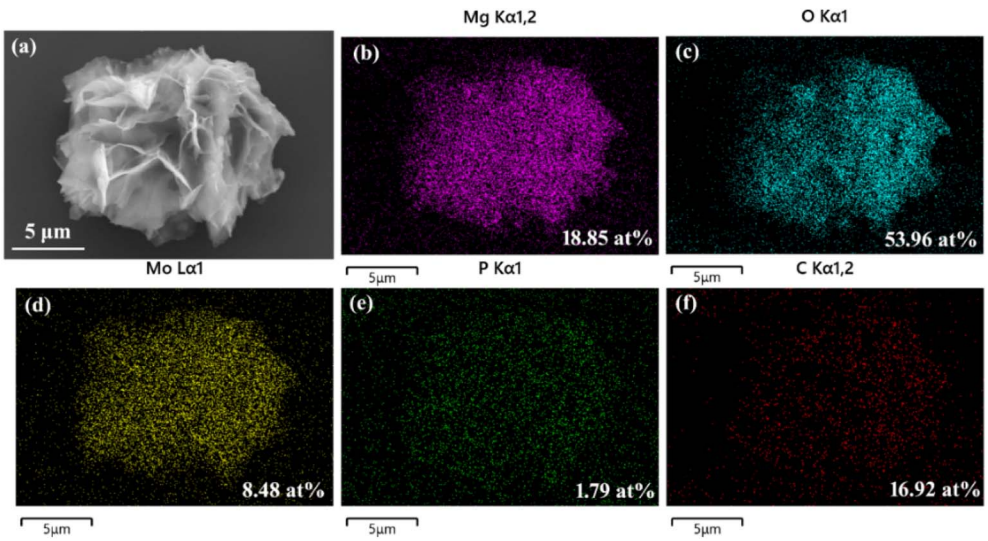

Fig. 2 SEM images (a) and elemental distribution images of MO@MH-PEPE: (b) Mg, (c) O, (d) Mo, (e) P, and (f) C.

previously reported multi-component flame retardant),[33] this system shows reduced Mg and C content with increased O content, which is attributed to the MoO_3 incorporation within the MO@MH. The particle size distribution curves of MO@MH and MO@MH-PEPE are shown in Fig. S4. Compared with MO@MH, MO@MH-PEPE also exhibits a primary particle size distribution in the range of 1–10 μm. However, the proportion of particles in the 0.1–1 μm range increases while the fraction of particles in the 10–100 μm range decreases. This indicates that PEPE modification effectively suppresses the aggregation behavior of MO@MH and improves its dispersibility.

XPS was used to further analyze the varieties and states of different elements in MO@MH-PEPE, as shown in Fig. 3. As shown in the C1s high-resolution spectrum of MO@MH-PEPE, the peak at 284.8 eV is attributed to C–C/C–H bond, the peak at 286.4 eV is attributed to C–O bond.[34] As shown in the O 1s high-resolution spectrum of MO@MH-PEPE, it can be divided into two peaks of 530.9 eV and 533.1 eV, which are respectively attributed to lattice oxygen (O–Mg bond) and O–C/P bond. In the Mo 3d spectrum of MO@MH-PEPE, Mo^{+6} ($3d_{3/2}$) at 235.7 eV and Mo^{+6} ($3d_{5/2}$) at 232.6 eV appear,[35] indicating that the molybdenum element in the filler mainly exists in a hypervalent state. The most significant change is in the P 2p spectrum, the P–O/P═O (133.6 eV) bond appears on MO@MH-PEPE,[36] indicating that there is physical adsorption or chemically bonded PEPE on MO@MH-PEPE.

3.2 Thermal degradation behavior of flame retardants and fPVC composites

In order to systematically evaluate the thermal stability of MH, MO@MH and MO@MH-PEPE, thermogravimetric analysis (TGA) and differential thermogravimetric analysis (DTG) were used to characterize them under a nitrogen atmosphere. The results are presented in Fig. 4(a) and (b). The key thermal decomposition parameters are summarized in Table S1. As shown in Fig. 4(a), MO@MH and MO@MH-PEPE transform the original single-step decomposition process of MH into a two-step decomposition. Specifically, MH exhibits an initial decomposition temperature (T_{05}) of 343.3 °C, a maximum decomposition rate temperature (T_{peak}) of 375.8 °C, and a maximum decomposition rate of 0.57% min^{-1}, showing characteristics of intense decomposition and poor thermal stability. The residual rate is 69.0% at 800 °C. In contrast, the T_{05} of MO@MH reduces 271.1 °C due to the catalytic action of MoO_3. However, the final residual rate of MO@MH increases significantly to 85.5%. After modification of PEPE, the T_{05} of MO@MH-PEPE further decreases to 208.5 °C, which may be attributed to the poor thermal stability of PEPE itself and the synergistic catalytic effect of MoO_3. The residual rate at 800 °C is still as high as 85.7%, indicating that the charring ability was not affected.

The thermal stability of the fPVC composite was also evaluated by TGA and DTG analysis, and the results are shown in Fig. 4(c), (d) and Table 2. All samples exhibited typical two-step thermal decomposition behavior, corresponding to PVC dechlorination and carbon chain skeleton decomposition respectively. Compared with fPVC, the T_{05} of fPVC composites increased with the addition of MH, MO@MH and MO@MH-PEPE. For instance, the T_{05} of fPVC/MO@MH-PEPE reaches 257.5 °C, indicating the enhancement of thermal stability. This improvement can be attributed to the thermal dilution and physical barrier effect provided by MO@MH, and the inhibition

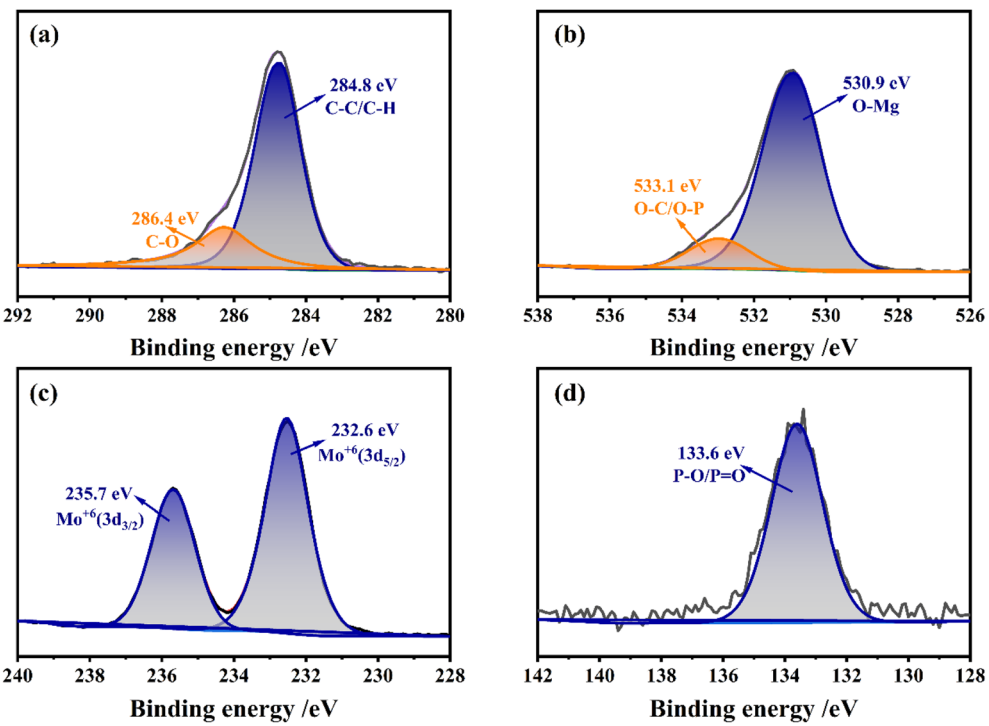

Fig. 3 XPS high-resolution spectra of MO@MH-PEPE: (a) C 1s, (b) O 1s, (c) Mo 3d, and (d) P 2p.

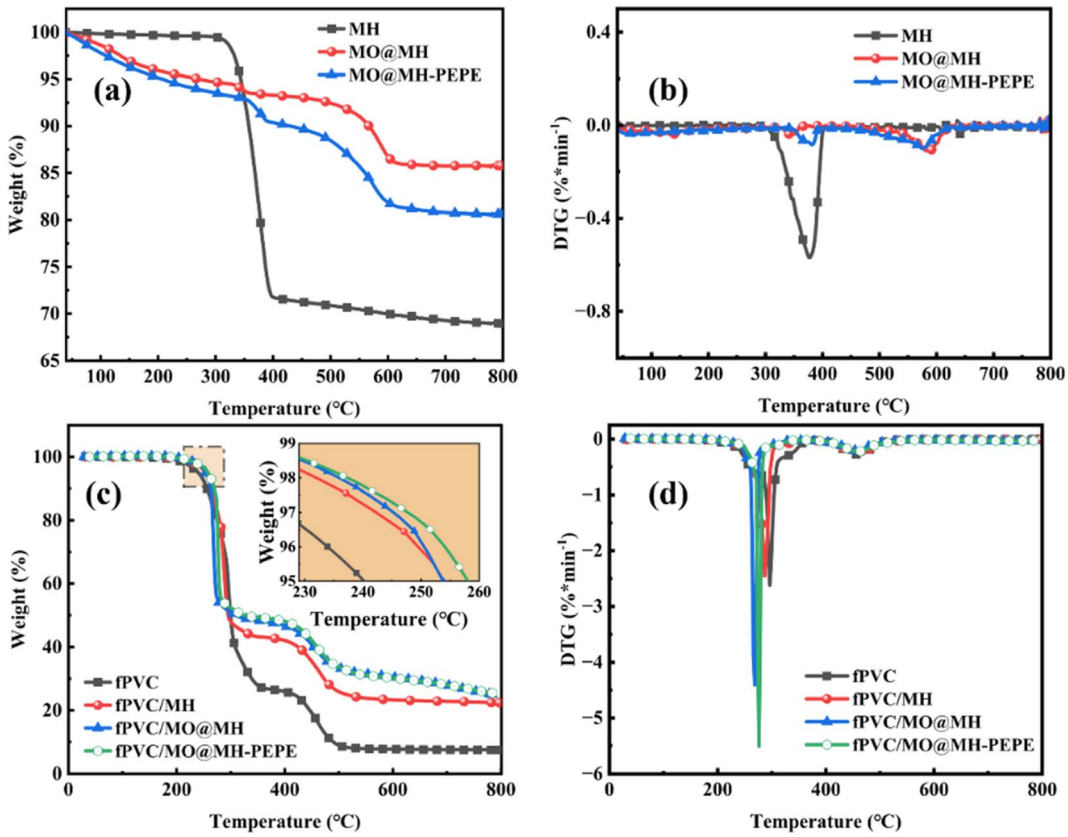

Fig. 4 TG and DTG results of (a) and (b) MH, MO@MH and MO@MH-PEPE (c) and (d) fPVC, fPVC/MH, fPVC/MO@MH and fPVC/MO@MH-PEPE in N_2 atmosphere.

Table 2 TGA data for fPVC and fPVC composites[a]

Sample	T_{05} (°C)	T_{peak} (°C)	Residue (%)
fPVC	240.2	296.4	7.9
fPVC/MH	253.8	287.1	22.4
fPVC/MO@MH	253.8	268.8	25.0
fPVC/MO@MH-PEPE	257.5	276.6	25.5

[a] T_{05}: temperature at 5 wt% mass loss; T_{peak}: maximum decomposition rate temperature.

of thermal decomposition reaction by improved interfacial compatibility after PEPE modification. In addition, the residual rates of fPVC/MO@MH and fPVC/MO@MH-PEPE at 800 °C are 25.0% and 25.5%, respectively, which are significantly higher than fPVC (9.7%) and fPVC/MH (22.4%), further proving the good thermal stability and charring promotion ability.

3.3 Flame retardant properties of fPVC composites

To systematically evaluate the flame-retardant and smoke-suppression efficiency of the magnesium–molybdenum–phosphorus multi-component flame retardant in fPVC composites, four systems, fPVC, fPVC/MH, fPVC/MO@MH andfPVC/MO@MH-PEPE composites, were selected for comparative analysis. Quantitative assessments were performed through UL 94 vertical burning tests, LOI measurements, and cone calorimetry analysis. Fig. 5 shows the photos of the UL 94 vertical burning tests. Pure fPVC material showed poor flame retardancy, the sample continued to burn for about 3 s after the first ignition, and violently burned for about 2 s after the second ignition, accompanied by obvious melting and dripping phenomenon, ignited cotton, and was rated as V-2. As mentioned in the previous work, the fPVC/MH composite was extinguished at about 1 s and 13 s after the first and second ignition, respectively. No molten droplets were observed during the burning process, which meant a V-1 rating was achieved for it. In contrast, both the fPVC/MO@MH and fPVC/MO@MH-PEPE composites demonstrated markedly enhanced combustion resistance. These two composites were immediately extinguished within 2–4 s after the first and second ignition and no molten droplets were observed during the burning process. Hence, both the fPVC/MO@MH and fPVC/MO@MH-PEPE composites passed the V-0 rating in UL 94 vertical burning tests.

The LOI, quantified as the minimum oxygen concentration (vol%) required to sustain candle-like combustion in an O_2/N_2 mixture, serves as a critical indicator of material flammability. As documented in Table 3, the LOI value of pure fPVC is 24.0%, showing poor flame retardant properties. The fPVC/MH composite exhibited an LOI value of 29.7%, whereas the fPVC/MO@MH and fPVC/MO@MH-PEPE composites demonstrated elevated LOI values of 31.0% and 32.0%, respectively. Therefore, it is preliminary confirmed that the magnesium–molybdenum–

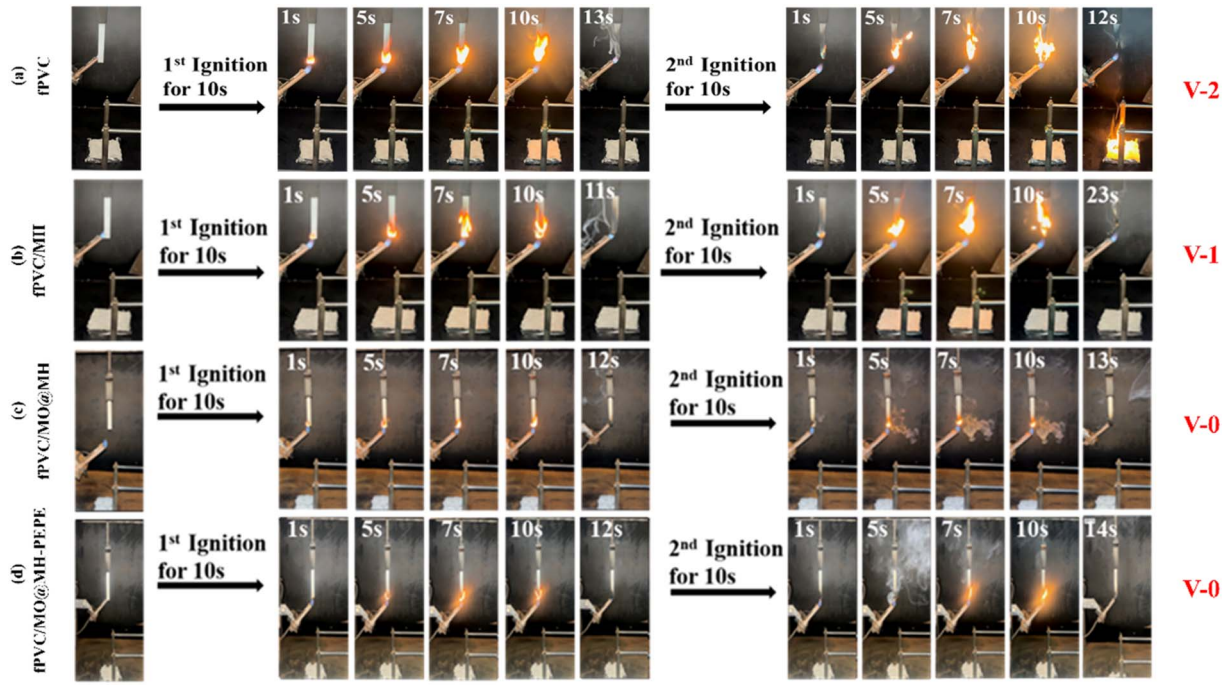

Fig. 5 Photos of UL 94 tests for the fPVC (a), fPVC/MH (b), fPVC/MO@MH (c), and fPVC/MO@MH-PEPE composites (d).

phosphorus multi-component flame retardant performed better than MO@MH and MH in flame retardant fPVC.

Fig. 6 shows the cone calorimetry tests results of fPVC, fPVC/MH, fPVC/MO@MH, and fPVC/MO@MH-PEPE composites, including heat release rate (HRR), total heat release (THR), smoke production rate (SPR), and total smoke production (TSP) curves. The corresponding data are summarized in Table 3. As shown in Fig. 6(a), the incorporation of MO@MH and MO@MH-PEPE results in moderated HRR curves for fPVC composites. According to Table 3, the peak HRR (pHRR) values of fPVC/MO@MH and fPVC/MO@MH-PEPE composites are 139.91 and 133.80 kW m^{-2}, respectively. These values represent a reduction of 58.48% and 60.29% compared to pure fPVC (337.01 kW m^{-2}) and a decrease of 44.74% and 47.16% compared to fPVC/MH composites (257.33 kW m^{-2}), respectively. These data confirmed that the introduction of MO@MH and MO@MH-PEPE significantly reduced the pHRR value of fPVC composites, among which MO@MH-PEPE composite system showed better heat release inhibition effect, further verifying the effectiveness of its synergistic flame retardant mechanism in inhibiting heat release rate. Consistent conclusions emerge from the THR curves in Fig. 6(b), where the THR of the fPVC/MO@MH-PEPE composite is reduced by 29.54% and 31.59% compared to pure fPVC and fPVC/MH composites. In addition to these, the fPVC/MH and fPVC/MO@MH composites show almost the same time to ignition (TTI), while the TTI of fPVC/MO@MH-PEPE composite increases significantly to 68 s, indicating enhanced ignition resistance that holds practical implications for fire safety applications.

Particular emphasis was placed on smoke production analysis of PVC composites, as PVC combustion inherently produces toxic fumes whose asphyxiating effects constitute the primary cause of fire-related fatalities. Fig. 6(c) reveals significant reduction of SPR curves in fPVC composites following the incorporation of MO@MH and MO@MH-PEPE. As quantified in Table 3, the peak SPR (pSPR) values of the fPVC/MO@MH and fPVC/MO@MH-PEPE composites were 0.0234 m^2 s^{-1} and 0.0415 m^2 s^{-1}, respectively, representing reductions of 90.02% and 82.30% compared to pure fPVC (0.2345 m^2 s^{-1}). When compared with the fPVC/MH composite (0.1007 m^2 s^{-1}), the reductions were 76.76% and 58.79%, respectively. This confirms the superior smoke suppression ability of both MO@MH and MO@MH-PEPE over MH. The discrepancy of smoke suppression between MO@MH and MO@MH-PEPE is

Table 3 CCT data of fPVC, fPVC/MH, fPVC/MO@MH and fPVC/MO@MH-PEPE composites

Sample	TTI (s)	pHRR (kW m^{-2})	THR (MJ m^{-2})	pSPR (m^2 s^{-1})	TSP (m^2)	Residue (wt%)	LOI (%)
fPVC	33	337.01	51.82	0.2435	30.34	14.44	24.0
fPVC/MH	30	253.20	53.37	0.1007	10.86	30.81	29.7
fPVC/MO@MH	29	139.91	39.31	0.0234	4.93	46.21	31.0
fPVC/MO@MH-PEPE	68	133.80	36.51	0.0415	2.70	50.00	32.0

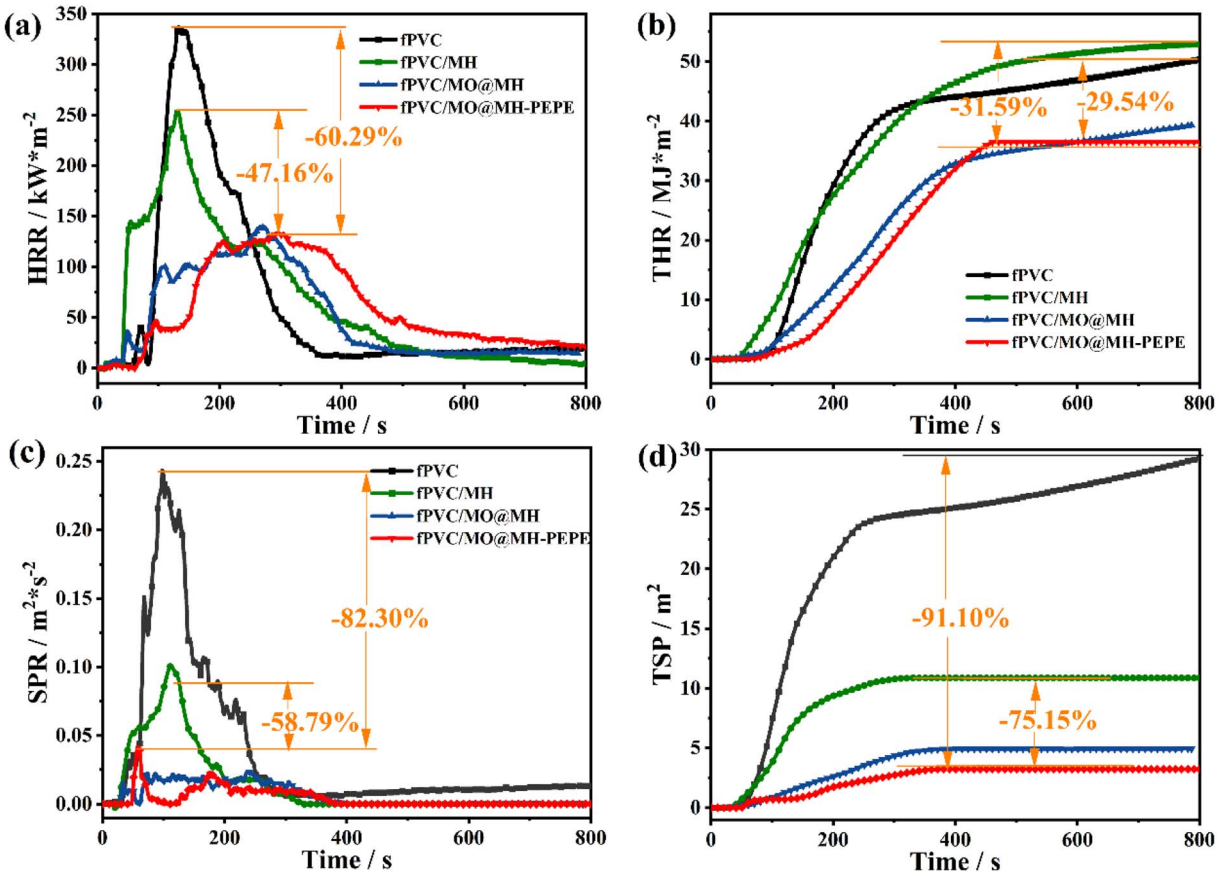

Fig. 6 HRR (a), THR (b), SPR (c) and TSP (d) curves of fPVC, fPVC/MH, fPVC/MO@MH, and fPVC/MO@MH-PEPE composites.

further elucidated in Fig. 6(d). The data in Table 3 reveal a TSP reduction from 10.86 m^2 (fPVC/MH composite) to 4.93 m^2 (fPVC/MO@MH composite), with fPVC/MO@MH-PEPE composite achieving an exceptional 75.15% decrease to 2.70 m^2. The enhanced smoke suppression correlates with char residue characteristics: fPVC/MO@MH-PEPE exhibits a 50.00% char yield, substantially higher than other composites. Mechanistically, the improvement in flame retardancy can be attributed to synergistic carbonization catalysis between phosphorus-containing species (*e.g.* phosphoric acid, pyrophosphoric acid and metaphosphoric acid) generated during PEPE decomposition and molybdenum oxide nanoparticles from MoO_3, which is consistent with previous studies.[32] In summary, the introducing of magnesium–molybdenum–phosphorus multi-component flame retardant can effectively improve the flame-retardant and smoke–suppression properties of fPVC composites.

3.4 Flame retardant mechanism

3.4.1 Condensed phase mechanism. The char residue was analyzed in detail, and its appearance was shown in Fig. S5 and 7. As shown in Fig. S5(a1) and (a2), the char residue of fPVC after combustion is black, the surface is rough, the structure is loose and the morphology is irregular, and the mechanical strength of the char layer is extremely low. From Fig. S5(b1) and (b2), it can be seen that the char residue of fPVC/MH composite is composed of messy and broken grayish-white substances, and its structure can be destroyed into powdering substances by slight touch. In contrast, as shown in Fig. S5(c1) and (c2), the char residue of fPVC/MO@MH composite has a more complete structure. The external surface of fPVC/MO@MH composite is white concave and convex, showing obvious expansion effect, and the hardness is obviously better than that of fPVC/MH composite. Obviously, this outer surface structure is more conducive to blocking the transfer of combustible volatiles and heat during the combustion process. In fPVC/MO@MH-PEPE as shown in Fig. 7(a) and (b), the introduction of PEPE further optimizes the structure of char residue, making it dense and flat, and significantly increasing its thickness, thus effectively isolating heat, oxygen and combustible volatiles, which is an important reason for its excellent flame retardant and smoke suppression performance. According to the data of Table 3, the char yield of fPVC/MO@MH-PEPE composite reaches 50.00 wt%, which is 62.3% higher than that of fPVC/MH composite. This significant difference indicates that the introduction of MO@MH-PEPE has a double effect on the carbonization process of the fPVC matrix promoting effect: on the one hand, the char yield is significantly increased. On the other hand, the structural integrity and stability of the char residue are improved. This kind of the efficient charring mechanism can be attributed to the synergistic catalytic action between

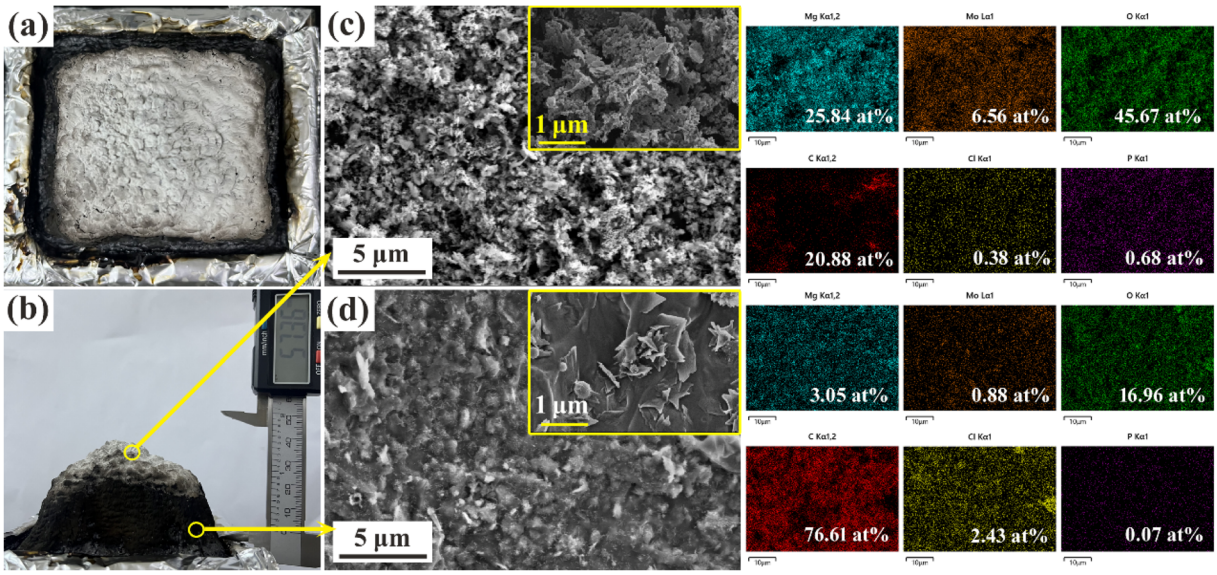

Fig. 7 Photos of char residues of the fPVC/MO@MH-PEPE composites (a) and (b); SEM and EDS images of the outer (c) and inner (d) char residues of the fPVC/MO@MH-PEPE composites.

magnesium, molybdenum and phosphorus elements, which forms excellent thermal barrier property of the char layer structure.

Fig. 7(c) and (d) show the SEM images of the inner and outer char residues of the fPVC/MO@MH-PEPE composite. Fig. 7(c) display the outer char layer, which presents an aggregate structure composed predominantly of granular particles with minor blocky fragments. This layer exhibits a relatively loose structure containing numerous pores, cracks, and defects that allow gas permeation. As shown in Fig. 7(d), the inner char layer exhibits a compact and continuous structure without visible pores. Lamellar-like structures, presumably the decomposition product of MO@MH-PEPE filler, are distinctly observable on the surface and are well integrated with the char matrix. This indicates that the synergistic effect of MO@MH and PEPE significantly enhances the formation of a dense and stable char layer during combustion. This structure is similar to a "labyrinth" barrier path. This structure not only improves the insulation ability of heat and oxygen, but also significantly prolongs the diffusion path of combustible gases, thus effectively inhibiting the release of volatile combustible decomposition products. The distinct structural characteristics of the inner and outer layers indicate a dual protective mechanism: the outer char layer provides an initial thermal barrier *via* expansion, while the inner char layer further impedes the transfer of heat and flammable gases. This combined action effectively decreases the fPVC matrix from thermal decomposition, thereby significantly enhancing the flame retardancy and smoke suppression properties.

EDS element distribution analysis was performed on the char residues of the inner and outer layers of the fPVC/MO@MH-PEPE composite (Fig. 7). The EDS data for the outer char layer reveal that the predominant elements are Mg (25.84 at%), O (45.67 at%), and C (20.88 at%), with minor amounts of Mo (6.56 at%), Cl (0.38 at%), and P (0.68 at%). This composition indicates that the outer char residue is primarily composed of inorganic compounds such as MgO and MoO_3. In contrast, the inner char layer exhibits a significantly higher C content (76.61 at%), suggesting it is predominantly comprised of a carbonaceous structure. Concurrently, the contents of O, Mg, Mo, and P are substantially reduced, demonstrating a decrease in MO@MH-PEPE within the inner layer. This implies that MO@MH-PEPE migrated towards the composite's outer surface during combustion. Obviously, the P content in the inner layer decreased markedly to 0.07 at%. This effective char formation promoted by the low P content is considered a key factor contributing to the structural integrity and stability of the char residue.

To quantitatively characterize the compactness of the residues, which is crucial for condensed-phase flame retardancy, Raman spectroscopy was performed on the inner-layer residues of the fPVC/MH, fPVC/MO@MH, and fPVC/MO@MH-PEPE composites, as shown in Fig. 8. The Raman spectra reveal that all three residues exhibit characteristic D and G bands located at approximately 1370 cm^{-1} and 1580 cm^{-1}, corresponding to amorphous carbon and graphitic carbon, respectively. The ratio of the integrated areas of these two bands, denoted as I_D/I_G, is commonly used to evaluate the graphitization degree of the residue.[37,38] A lower I_D/I_G value indicates a higher graphitization degree. Based on peak deconvolution and fitting calculations, the I_D/I_G value for the fPVC/MH composite residue is 2.67. In contrast, the values for the fPVC/MO@MH and fPVC/MO@MH-PEPE residues decrease to 1.65 and 1.38, respectively. These results demonstrate that both the introduction of MO hybridization and the PEPE modifier effectively enhance the graphitization degree of the residue. The fPVC/MO@MH-PEPE composite residue exhibits the highest graphitization degree,

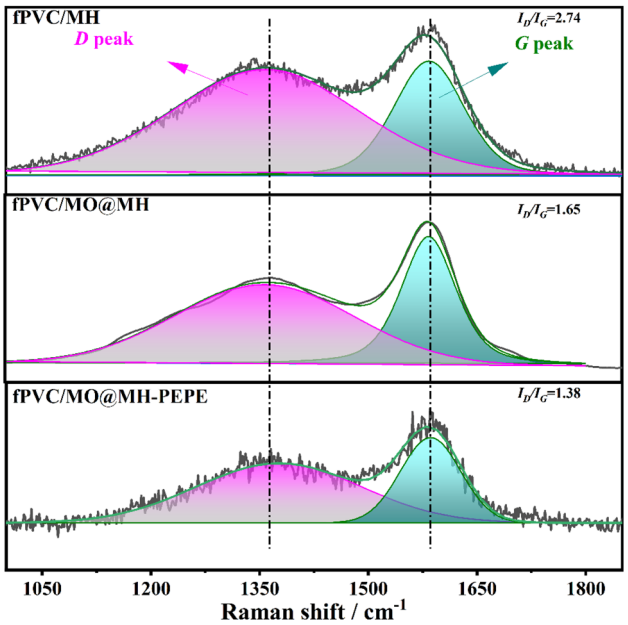

Fig. 8 Raman spectra of the inner char residues of fPVC/MH, fPVC/MO@MH and fPVC/MO@MH-PEPE composites.

which is a key factor contributing to its superior flame retardancy and smoke suppression performance.

The XPS high-resolution spectra of the inner char residue from the fPVC, fPVC/MH, fPVC/MO@MH, and fPVC/MO@MH-PEPE composite are presented in Fig. 9 and S6. As revealed in Fig. 9(a), the C1s spectrum can be deconvoluted into three peaks at 284.0, 284.8, and 286.0 eV, assigned to C=C, C–C/C–H, and C–O bonds, respectively. The carbon atoms in both C–C/C–H and C–O bonds exhibit sp^3 hybridization, likely originating from the PVC matrix itself. Significantly, the appearance of the C=C bond indicates the presence of sp^2-hybridized carbon atoms, confirming graphitic carbon formation. In other words, the inner char residue of fPVC/MO@MH-PEPE demonstrates a distinct graphitization tendency, consistent with the Raman spectroscopy results discussed earlier. In comparison, the C 1s spectra of fPVC and fPVC/MH composites are deconvolved into other three characteristic peaks at 284.8, 286.2 and 289.2 eV, corresponding to C–C/C–H, C–O, and O–C=O bonds, respectively, as shown in Fig. S6. Simultaneously, the C=C characteristic peak at 284.0 eV still appears in the C 1s spectrum of fPVC/MO@MH composite. Hence, it is confirmed that the introduction of MO@MH can promote the formation of

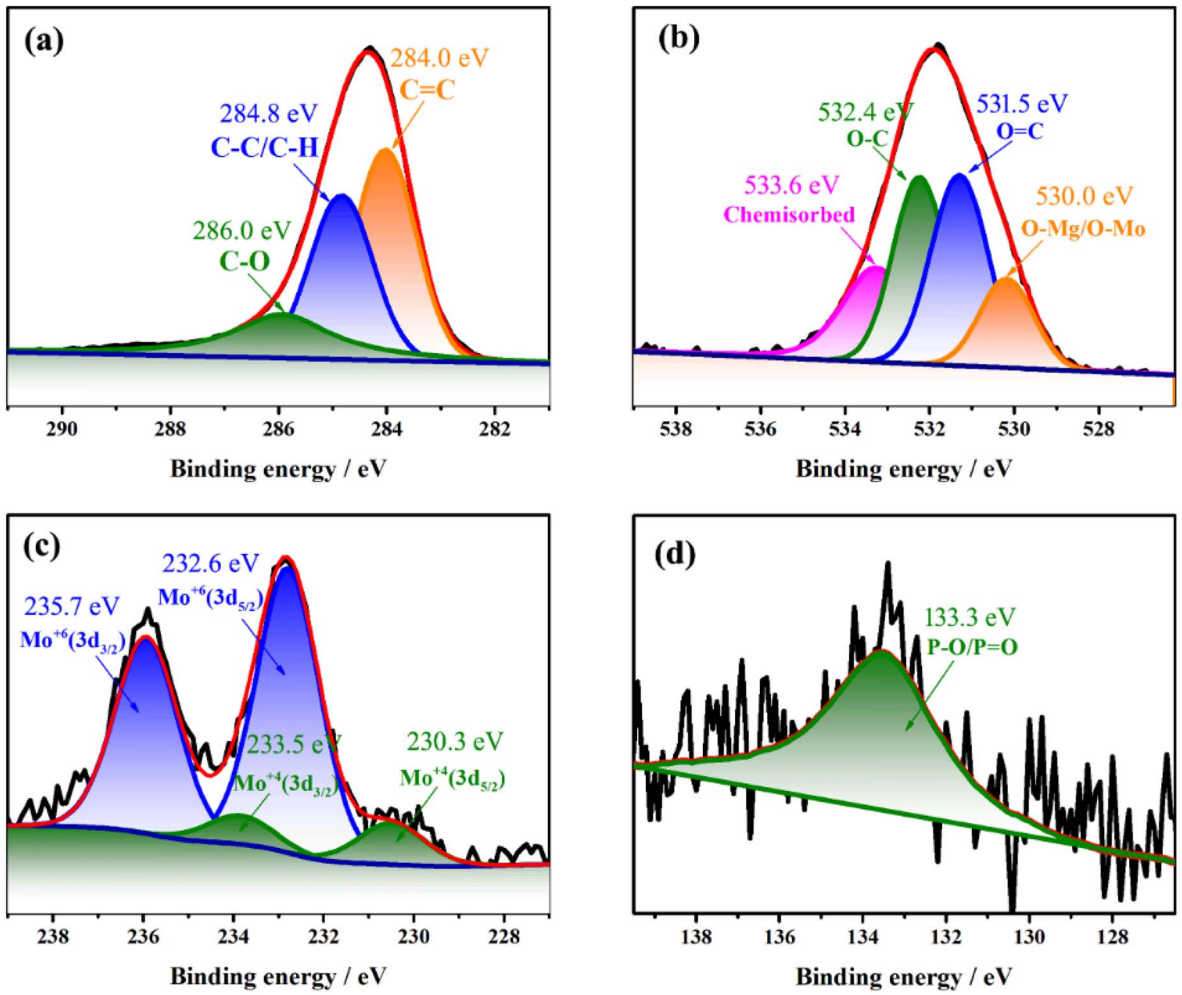

Fig. 9 XPS high-resolution spectra of the inner char residues of fPVC/MO@MH-PEPE composites: (a) C 1s, (b) O 1s, (c) Mo 3d, and (d) P 2p.

graphitized carbon during combustion, and the addition of PEPE can further strengthen this graphitization trend Fig. 9(b) displays the O 1s spectrum, resolved into four peaks at 530.0, 531.5, 532.4, and 533.6 eV, corresponding to lattice oxygen (O–Mg or O–Mo bonds), O–C/O–P bonds, O═C/O═P bonds, and chemically adsorbed oxygen, respectively. Compared to MO@MH-PEPE, the Mo 3d spectrum in Fig. 9(c) exhibits notable changes. In addition to the peaks at 235.7/232.6 eV attributed to Mo^{6+}, weaker peaks emerge at 233.5/230.3 eV, indicating partial reduction of Mo^{6+} to Mo^{4+}.[33,34] It is further indicated that MoO_3 phase in the filler is involved in the carbonization process of fPVC matrix in the form of redox reaction. In contrast, XPS analysis of fPVC/MO@MH-PEPE shows some significant changes, with a P–O/P═O (133.3 eV) characteristic peak detected in the P 2p spectra, which is attributed to the large presence of PEPE's own structure and the creation of more P═O/P–O bonds during combustion.

3.4.2 Gas phase mechanism. The flame retardant mechanism of MO@MH PEPE in gas phase was analyzed by TGA-FTIR. Fig. S7 shows the three-dimensional infrared spectra of fPVC

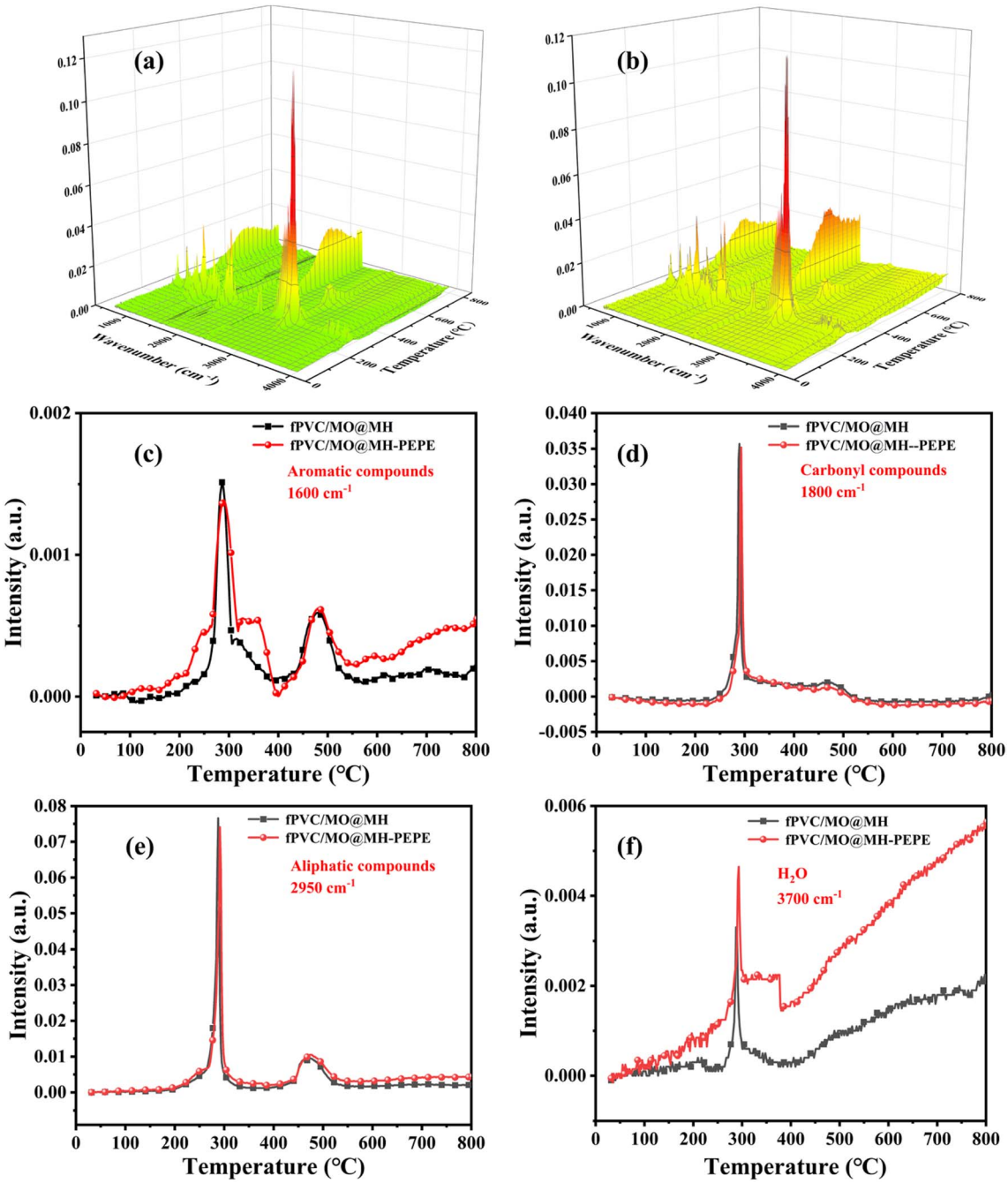

Fig. 10 (a) 3D infrared spectra of fPVC/MO@MH and (b) fPVC/MO@MH-PEPE composites; the intensity changes of (c) aromatic compounds, (d) carbonyl compounds, and (e) aliphatic compounds, (f) H_2O produced by cracking.

and fPVC/MH. By further comparing the TGA-FTIR three-dimensional spectra of fPVC/MO@MH and fPVC/MO@MH-PEPE composites in Fig. 10 with the intensity change curves of pyrolysis products (Fig. 10(a)–(e)), it is found that they are basically consistent in the types and evolution trends of gaseous decomposition products. Both spectra exhibit the following characteristic peaks: aliphatic compounds (C–H stretching vibrations at 3000–2800 cm^{-1} and C–H bending vibrations at 1300–1000 cm^{-1}), carbonyl compounds (C=O stretching vibrations at 1800–1650 cm^{-1}),[39,40] and aromatic compounds (C=C aromatic ring vibrations at 1600–1450 cm^{-1}).[41] The generation of these substances is associated with the dehydrochlorination reaction and backbone scission of the PVC matrix. Further analysis of Fig. 10(c)–(e) shows that although PEPE modification does not significantly change the species and release trends of these gaseous products, their characteristic peak intensities are slightly reduced. It is interesting to note that in Fig. 10(f), the H_2O absorption peak intensity of fPVC/MO@MH-PEPE composite in the region of 3500–4000 cm^{-1} is significantly enhanced,[42] indicating that this material releases more water vapor during pyrolysis to dilute the combustible gas concentration in the combustion region and inhibit flame propagation. To sum up, the gas phase flame retardant mechanism of fPVC/MO@MH-PEPE composites is mainly reflected in the dilution of water vapor.

3.4.3 Flame-retardant mechanisms. Based on the above analysis, the possible flame-retardant mechanism of the Mg–Mo–P multi-component flame retardant is inferred, as detailed in Fig. 11. In the condensed phase, MgO generated from the thermal decomposition of MO@MH primarily resides on the composite surface, forming a fragile outer char layer that is ineffective at hindering the transfer of heat and flammable volatiles, while another portion of MgO combines with carbonaceous or carbon–oxygen compounds to ultimately form a hard, continuous, and dense inner char layer that effectively shields the underlying matrix from flammable free radicals and heat. During this process, part of the MoO_3 utilizes its Lewis acid catalytic effect to catalyze char formation within the PVC matrix, concurrently undergoing reduction from the +6 oxidation state to +4. Additionally, the thermal dehydration of the PEPE coating on the MO@MH surface generates acids such as phosphoric acid, metaphosphoric acid, and pyrophosphoric acid, whose catalytic action significantly enhances the integrity, compactness, and total yield of the char residue. In the gas phase, water vapor reduces the concentration of oxygen and combustible volatiles by dilution. At the same time, the pyrolysis of PEPE produces phosphorus radicals (such as $P^{\bullet}$, $PO^{\bullet}$, $PO_2^{\bullet}$), which can efficiently capture $H^{\bullet}$ and $HO^{\bullet}$ radicals after entering the flame region, thus interrupting the combustion chain reaction and inhibiting the propagation of flame.[43–46]

3.5 Mechanical properties of fPVC composites

Fig. 12 displays the tensile strength and impact strength of the fPVC, fPVC/MH, fPVC/MO@MH, and fPVC/MO@MH-PEPE composites. As shown in Fig. 12(a) and (b), the tensile strength of fPVC was 19.33 MPa, and the tensile strength of fPVC/MH composites decreased to 16.32 MPa after MH addition, while the tensile strength of fPVC/MO@MH composites decreased further to 12.77 MPa after MO@MH addition. This indicates that the MO@MH filler provides less reinforcement to the fPVC matrix compared to MH. The primary reason for this phenomenon is that MO@MH consists of a flake-assembled microflower structure. Compared to flaky MH, MO@MH possesses a more complex structure and larger size. Without any surface modification treatment, defects are more likely to form at the interface between MO@MH and the fPVC matrix. Fig. 12(g) shows a poorly compatible interface of fPVC/MO@MH composite. Under tensile stress, this interface is more prone to debonding, leading to stress concentration and premature fracture. In contrast, the tensile strength of the fPVC/MO@MH-PEPE composite reaches 16.39 MPa. This value is not only significantly higher than that of the fPVC/MO@MH composite but also slightly exceeds that of the fPVC/MH composite. This

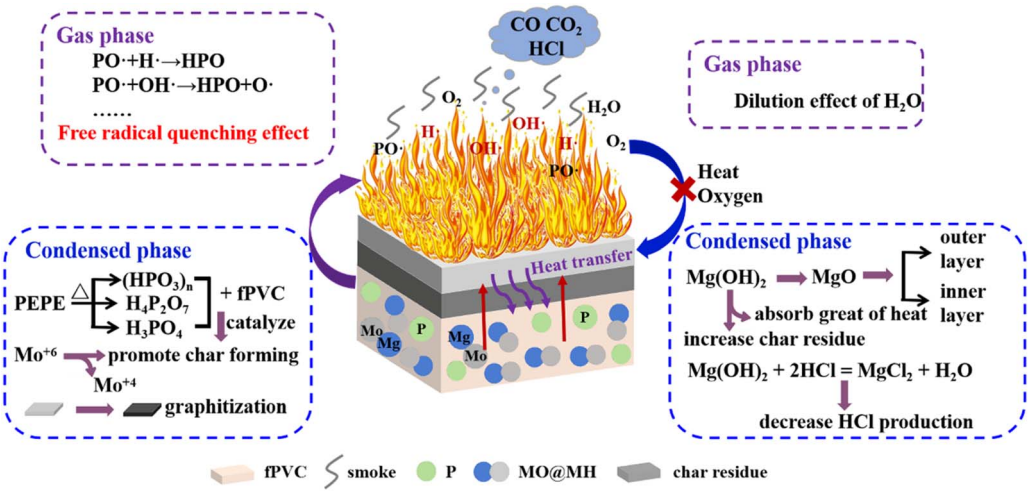

Fig. 11 Schematic illustration of the mechanism for the enhanced flame resistance and smoke suppression of the fPVC/MO@MH-PEPE composite.

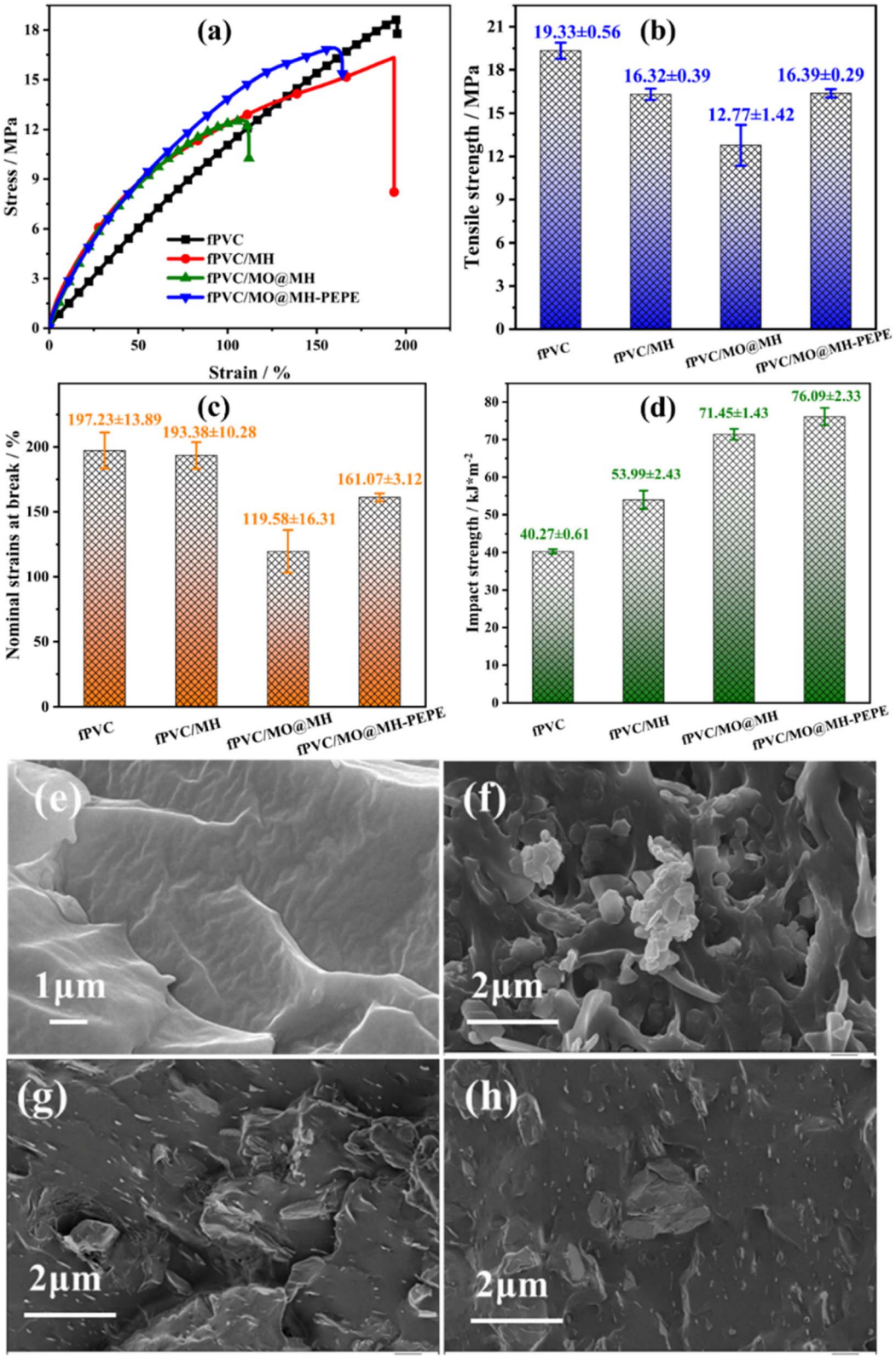

Fig. 12 Stress–strain curves (a), tensile strength (b), nominal strains at break (c), and impact strengths (d) of fPVC, fPVC/MH, fPVC/MO@MH and fPVC/MO@MH-PEPE composites; SEM images of cryo-fractured fPVC (e), fPVC/MH (f), fPVC/MO@MH (g), and fPVC/MO@MH-PEPE (h) composites.

demonstrates that PEPE modification improves the interfacial compatibility between MO@MH and fPVC, enhances interfacial interactions, and consequently facilitates more effective stress transfer, as shown in Fig. 12(h). In Fig. 12(c), the nominal strain at break of fPVC was 197%, and decreased slightly to 193.38% after adding MH. The nominal strain at break of fPVC/MO@MH and fPVC/MO@MH-PEPE composites was lower than that of fPVC/MH, indicating that the introduction of MO@MH reduced the ductility of the composites to some extent. However, this parameter is also enhanced to 161.07% for the fPVC/MO@MH-PEPE composite in comparison with the fPVC/MO@MH composite.

The impact strengths of fPVC, fPVC/MH, fPVC/MO@MH, and fPVC/MO@MH-PEPE composites shown in Fig. 12(d) are 40.27, 53.99, 71.45, and 76.09 kJ m^{-2}, respectively. The fPVC/MO@MH-PEPE composite again exhibits the best performance. The impact strength of the fPVC/MO@MH composite is 23.77% higher than that of the fPVC/MH composite. Furthermore, the introduction of the PEPE modifier further increased the impact strength to 76.09 kJ m^{-2} for the fPVC/MO@MH-PEPE composite. Both the fPVC/MO@MH and fPVC/MO@MH-PEPE composites exhibit significantly higher impact strength than the fPVC/MH composite. As discussed earlier, the introduction of the PEPE modifier improves the interfacial compatibility and enhances the interfacial interactions between the MO@MH filler and the fPVC matrix. Consequently, more energy is required to separate MO@MH from the fPVC matrix under external impact. All the above results indicate that PEPE modification effectively enhances the mechanical properties of the fPVC/MO@MH composite.

4 Conclusions

This study demonstrates that surface modification of self-synthesized molybdenum oxide-hybridized magnesium hydroxide (MO@MH) with phenolic epoxy phosphate ester (PEPE) successfully constructs a magnesium–molybdenum–phosphorus ternary flame retardant (MO@MH-PEPE), which significantly enhances the fire safety and mechanical properties of flexible PVC composites. Structural characterization (FTIR/XPS/SEM-EDS) confirms the formation of P–O–Mg covalent bonds and uniform dispersion of elements (Mg, Mo, P). The fPVC/MO@MH-PEPE composite achieves outstanding flame retardancy (LOI of 32.0%, UL-94 V-0 rating, 47.16% reduction in pHRR) and exceptional smoke suppression (75.15% reduction in TSP *versus* fPVC/MH), attributed to the synergistic catalytic charring effect involving $Mo^{6+} \rightarrow Mo^{4+}$ redox reactions and phosphoric acid generation from PEPE, forming a dense bilayer char residue (50.00 wt% yield, $I_D/I_G = 1.38$ graphitization) that effectively blocks heat and mass transfer. Remarkably, PEPE modification simultaneously improves interfacial compatibility, increasing tensile strength to 16.39 MPa (28.35% increase *versus* fPVC/MO@MH) and impact strength to 76.09 kJ m^{-2}, outperforming both MH and unmodified MO@MH composites. This work provides an effective strategy for developing high-performance fPVC composites through multi-element synergistic flame retardancy.

Author contributions

Xue Li and Xiaoyuan Liu are the co-first authors of this paper and have made equal contributions to the research work. Xue Li: data management, formal analysis, research and investigation, first draft writing. Xiaoyuan Liu: formal analysis, research investigation, raw data integration, result verification. Zhihui Lv: project guidance, visual presentation. Li Dang: funding support, methodological design, resource allocation, review and editing.

Conflicts of interest

The authors declare that they have no known competing financial interests or personal relationships that could have appeared to influence the work reported in this paper.

Data availability

The data supporting this article have been included as part of the SI.

Fig. S1: structural formula of PEPE. Fig. S2: XRD patterns of MO@MH. Fig. S3: SEM images of (a and b) MO@MH and (c and d) MO@MH-PEPE. Fig. S4: particle size distribution plot of MO @ MH and MO@ MH PEPE. Table S1: TG data for MH, MO@MH, MO@MH-PEPE. Fig. S5: Pphotographs of char residues of fPVC composites. Fig. S6: XPS high-resolution spectra of the inner char residues of fPVC, fPVC/MH and fPVC/MO@MH composites: (a) C 1s, (b) O 1s, (c) Mo 3d, and (d) P 2p. Fig. S7: (a) 3D infrared spectra of fPVC and (b) fPVC/MH composites. See DOI: https://doi.org/10.1039/d5ra04341g.

Acknowledgements

This work was financially supported by the National Natural Science Foundation of China (grant numbers: 22165024) and the Salt Lake Chemical Engineering Research Complex, Qinghai University (grant numbers: 2023-DXSSZZ-07).

References

1 Y. Li, L. Lv, W. Wang, J. Zhang, J. Lin, J. Zhou, M. Dong, Y. Gan, I. Seok and Z. Guo, Effects of chlorinated polyethylene and antimony trioxide on recycled polyvinyl chloride/acryl-butadiene-styrene blends: Flame retardancy and mechanical properties, *Polymer*, 2020, **190**, 122198.
2 A. E. Coman, A. R. Gabor, S. Stoian, C. A. Nicolae, V. Raditoiu, I. C. Gifu, T. V. Iordache and G. Hubca, New Formulations of Flame-retardant Flexible Polyvinylchloride Composites, *Mater. Plast.*, 2019, **56**, 568–577.
3 B. F. Qian, H. C. Zhu, P. F. Wang, P. P. Peng, J. N. Zhang, M. Y. Wu, J. Y. Liu, Q. Y. Wu and J. J. Yang, Synthesis, characterization and performance evaluation of different alkyl chain lengths flame-retardant plasticizers for poly(vinyl chloride) derived from sustainable vanillic acid, *Eur. Polym. J.*, 2024, **214**, 113154.

4 Q. Y. Song, H. J. Wu, H. Liu, T. Wang, W. H. Meng and H. Q. Qu, Chitosan-regulated inorganic oxyacid salt flame retardants: preparation and application in PVC composites, *J. Therm. Anal. Calorim.*, 2021, **146**, 1629–1639.

5 S. P. Chen, Z. R. Tan, Y. S. Qi and C. C. Ouyang, Sorption of tri-n-butyl phosphate and tris(2-chloroethyl) phosphate on polyethylene and polyvinyl chloride microplastics in seawater, *Mar. Pollut. Bull.*, 2019, **149**, 110490.

6 Y. L. Wang, N. Kang, J. Lin, S. X. Lu and K. M. Liew, On the pyrolysis characteristic parameters of four flame-retardant classes of PVC sheathless cable insulation materials, *J. Anal. Appl. Pyrolysis*, 2023, **170**, 105901.

7 L. Zhang, T. T. Chen, H. Xu, X. J. Liu, J. Zhang and R. D. Chai, Simultaneously enhanced flame retardancy and smoke suppression properties of flexible polyvinyl chloride with the incorporation of modified $Mg(OH)_2$ and Sb_2O_3, *Mater. Today Commun.*, 2023, **34**, 105448.

8 J. Gong, W. H. Guo, K. Wang and J. Y. Xiong, Surface modification of magnesium hydroxide sulfate hydrate whiskers and its toughness and reinforcement for polyvinyl chloride, *Polym. Compos.*, 2018, **39**, 3676–3685.

9 L. Dang, Z. H. Lv, X. L. Du, D. L. Tang, Y. T. Zhao, D. H. Zhu and S. A. Xu, Flame retardancy and smoke suppression of molybdenum trioxide doped magnesium hydrate in flexible polyvinyl chloride, *Polym. Adv. Technol.*, 2020, **31**, 2108–2121.

10 X. L. Chen, J. Yu, S. Y. Guo, S. J. Lu, Z. Luo and M. He, Surface modification of magnesium hydroxide and its application in flame retardant polypropylene composites, *J. Mater. Sci.*, 2009, **44**, 1324–1332.

11 X. J. Zhang, Z. D. Shao, T. T. Wei, X. G. Hou, X. M. Liu, J. W. Du and H. Deng, Alkali-Induced transformation of salt lake magnesium slag into novel magnesium hydroxide-coated aluminum hypophosphite nanomaterials and their synergistic flame retardant effects, *Surf. Interfaces*, 2025, **56**, 105745.

12 Y. H. Wang, W. H. Wu, G. Yang, Y. H. Jiao, H. Q. Qu and J. Z. Xu, Two kinds of activated carbon spheres-supported metal oxides for reducing smoke release volume and fire hazard in flexible poly(vinyl chloride), *J. Therm. Anal. Calorim.*, 2019, **135**, 2101–2110.

13 F. Guo, Y. Z. Zhang, L. Cai and L. J. Li, NiFe prussian blue analogue nanocages decorated magnesium hydroxide rod for enhancing fire safety and mechanical properties of epoxy resin, *Composites, Part B*, 2022, **233**, 109650.

14 T. T. Feng, J. H. Cui, M. Y. Ou, R. J. Li, Z. X. Zhao, Y. W. Geng, X. L. Chen and C. M. Jiao, 0D-2D nanohybrids based on binary transitional metal oxide decorated boron nitride enabled epoxy resin efficient flame retardant coupled with enhanced thermal conductivity at ultra-low additions, *Compos. Commun.*, 2023, **41**, 101649.

15 W. Cai, Y. L. Zhu, X. W. Mu, Z. X. Li, J. L. Wang, Y. Hu, X. Wang and L. Song, Heterolayered Boron Nitride/Polyaniline/Molybdenum Disulfide Nanosheets for Flame-Retardant Epoxy Resins, *ACS Appl. Nano Mater.*, 2021, **4**, 8162–8172.

16 F. Cheng, X. Zhu, F. Yun, M. Wei, C. Shi and J. Han, In-situ construction of BiOCl@Cu-MOF for synergistic flame retardancy, smoke suppression, and antibacterial properties in PVC coatings, *Prog. Org. Coat.*, 2025, **208**, 109504.

17 Q. Q. Bi, D. W. Yao, G. Z. Yin, J. Q. You, X. Q. Liu, N. Wang and D. Y. Wang, Surface engineering of magnesium hydroxide *via* bioinspired iron-loaded polydopamine as green and efficient strategy to epoxy composites with improved flame retardancy and reduced smoke release, *React. Funct. Polym.*, 2020, **155**, 104690.

18 G. F. Zeng, W. W. Zhang, X. Zhang, W. C. Zhang, J. X. Du, J. Y. He and R. J. Yang, Study on flame retardancy of APP/PEPA/MoO_3 synergism in vinyl ester resins, *J. Appl. Polym. Sci.*, 2020, **137**, 49026.

19 Z. S. Xu, H. Y. Jia, L. Yan, Z. Y. Chu and H. Zhou, Synergistic effects of organically modified montmorillonite in combination with metal oxides on the fire safety enhancement of intumescent flame-retarded epoxy resins, *J. Vinyl Addit. Technol.*, 2021, **27**, 161–173.

20 W. Z. Xu, C. C. Li, Y. X. Hu, L. Liu, Y. Hu and P. C. Wang, Synthesis of MoO_3 with different morphologies and their effects on flame retardancy and smoke suppression of polyurethane elastomer, *Polym. Adv. Technol.*, 2016, **27**, 964–972.

21 X. Y. Liu, X. Y. Bao, W. H. Liu, Y. K. Zheng, X. Li, Z. H. Lv and L. Dang, Nano-sized molybdenum trioxide doped magnesium hydroxide and its effect on flame retardancy and smoke suppression of flexible polyvinyl chloride, *Acta Mater. Compositae Sin.*, 2025, **42**, 4559–4573.

22 X. Yang, M. Y. Zhi, Y. C. Li, H. Xin, R. Fan, X. T. Chen, Q. Y. Liu and Y. H. He, Improved flame retardancy and smoke suppression properties of phenolic resin by incorporating MoO_3 particles, *High Perform. Polym.*, 2023, **35**, 559–570.

23 M. M. Yu, Z. M. Gao, W. Xie, X. C. Shi, O. S. Zhang, Z. G. Shen, L. Fang, M. S. Ren and J. L. Sun, A novel strategy utilizing oxidation states of phosphorus for designing efficient phosphorus-containing flame retardants and its performance in epoxy resins, *Polym. Degrad. Stab.*, 2024, **230**, 111016.

24 T. M. Zhang, H. Y. Xie, S. Xie, A. J. Hu, J. Liu, J. Kang, J. Hou, Q. Hao, H. Liu and H. X. Ji, A Superior Two-Dimensional Phosphorus Flame Retardant: Few-Layer Black Phosphorus, *Molecules*, 2023, **28**, 5062.

25 X. H. Li, Q. A. Xie, J. Y. Lin, J. T. Huang, K. L. Xie, J. C. Liu, X. J. Li and W. Wei, A phosphorus/silicon-containing flame retardant based on eugenol for improving flame retardancy and smoke suppression of epoxy resin, *J. Appl. Polym. Sci.*, 2023, **140**, e54474.

26 C. X. Yi, C. B. Xu, N. Sun, J. Xu, M. Ma, Y. Q. Shi, H. W. He, S. Chen and X. Wang, Flame-Retardant and Transparent Poly(methyl methacrylate) Composites Based on Phosphorus-Nitrogen Flame Retardants, *ACS Appl. Polym. Mater.*, 2022, **5**, 846–855.

27 L. Jia, W. C. Zhang, B. Tong and R. J. Yang, Crystallization, Mechanical and Flame-retardant Properties of Poly(lactic acid) Composites with DOPO and DOPO-POSS, *Chin. J. Polym. Sci.*, 2018, **36**, 871–879.

28 X. H. Zhang, F. Liu, S. Chen and G. R. Qi, Novel flame retardant thermosets from nitrogen-containing and phosphorus-containing epoxy resins cured with dicyandiamide, *J. Appl. Polym. Sci.*, 2007, **106**, 2391–2397.
29 H. Rupp, J. Ullmann, K. S. Shinde and A. Schadewald, Thiazole-based flame retardant for polyamide *vs.* a sulfur-free flame retardant with similar phosphorus and nitrogen content, *Mater. Chem. Phys.*, 2025, **329**, 130043.
30 X. Li, J. C. Zhang, X. Q. Yang, Y. K. Jin, Z. H. Lv, S. J. Lan, D. H. Zhu and L. Dang, Self-emulsification synthesis of epoxy phosphate ester and its flame-retardant mechanism in flexible poly(vinyl chloride)/magnesium hydroxide composites, *J. Appl. Polym. Sci.*, 2024, **141**, e55354.
31 X. Li, Y. K. Zheng, X. Y. Bao, J. Liu, W. H. Liu, X. Y. Liu and L. Dang, Synthesis of phosphorus-containing modifier based on phenolic epoxy resin and its application in flexible poly(vinyl chloride)/magnesium hydroxide composites, *Polym. Test.*, 2024, **140**, 108634.
32 L. Dang, X. Y. Nai, Y. P. Dong and W. Li, Functional group effect on flame retardancy, thermal, and mechanical properties of organophosphorus-based magnesium oxysulfate whiskers as a flame retardant in polypropylene, *RSC Adv.*, 2017, **7**, 21655–21665.
33 X. Y. Liu, J. Liu, W. Q. Ge, Z. H. Lv and L. Dang, Nano-architectured magnesium oxysulfate whisker decorated with scaly $Fe(OH)_3$ toward an efficient way to improving flame retardancy and smoke suppression of flexible polyvinyl chloride composites, *Polym. Degrad. Stab.*, 2025, **240**, 111446.
34 L. C. Xu, Q. Hu, Q. W. Ran, L. Li, G. Cai, H. J. Xie and X. Q. Liu, Mo^{6+} bifunctional substitution of P2-type manganese oxide for high performance sodium-ion batteries, *Chem. Eng. J.*, 2024, **493**, 152405.
35 Z. S. Zhan, S. H. Weng, T. Y. Bao, L. N. Yan, F. N. Meng and L. X. Li, Simultaneously boosting the flame retardancy and degradability of poly(lactic acid) composite by phosvitin affiliation, *Polym. Degrad. Stab.*, 2024, **230**, 111010.
36 X. W. Chen, S. P. Wang, S. Mahmud, J. Wang, J. Y. Dai and X. Q. Liu, Biobased hyperbranched flame retardant for epoxy resin modification: simultaneously improved flame retardancy, toughness, and smoke toxicity suppression, *Ind. Eng. Chem. Res.*, 2024, **63**, 20047–20058.
37 G. Wang, Q. He and K. Niu, One-step solution self-assembly synthesis of biomass-based flame retardants for constructing epoxy resins with superior flame retardant properties, *Constr. Build. Mater.*, 2025, **483**, 141706.
38 G. Q. Xiao, Z. W. Yang, C. L. Chen, C. Y. Chen, F. Zhong, M. T. Wang and R. Zou, Novel carbon nitride@polydopamine/molybdenum disulfide nanoflame retardant improves fire performance of composite coatings, *Colloids Surf., A*, 2021, **630**, 127575.
39 K. D. Qiu, X. D. Zhang, X. Y. Liu, Z. Q. Chen, L. Ni, Z. W. Chen, Y. Yu and J. C. Jiang, Enhancement of flame retardancy and mechanical properties of unsaturated polyester resin through organic-inorganic hybrid flame retardant composites, *React. Funct. Polym.*, 2025, **213**, 106266.
40 H. F. Chen, G. Z. Ji, F. Y. Lan, Z. Wang, C. Chen, J. X. Luan, C. H. Dong and Z. Lu, B/P/N flame retardant based on diboraspiro rings groups for improving the flame retardancy, char formation properties and thermal stability of cotton fabrics, *Int. J. Biol. Macromol.*, 2024, **270**, 132330.
41 Q. Jing, Y. H. Lu, Y. Yan, H. Zhou, J. H. Li, Y. Cheng and G. X. Zhang, A durable phosphorous-based flame retardant containing double reactive groups for cotton fabrics, *Polym. Degrad. Stab.*, 2024, **219**, 110616.
42 Q. Liu, J. Chu, Y. Xie, Z. Li, F. Wu, D. Feng, Y. Meng, Y. Mei and D. Xie, Novel Si-MXene/PAPP hybrid system for high-performance flame-retardant polypropylene composites, *Polym. Degrad. Stab.*, 2025, **239**, 111376.
43 H. Y. Ding, K. Huang, S. H. Li, L. N. Xu, J. L. Xia and M. Li, Flame retardancy and thermal degradation of halogen-free flame-retardant biobased polyurethane composites based on ammonium polyphosphate and aluminium hypophosphite, *Polym. Test.*, 2017, **62**, 325–334.
44 B. Huang, S. Ai, J. Tan, B. Zhou, Y. Pan, Z. Zheng, X. Ding and J. Deng, Enhancing Tensile Strength, Hydrophobicity, and Flame Retardancy of Epoxy Resin: π–π Stacking and Hydrogen Bonds, Fluorine, and Phosphorus–Fluorine Synergy, *ACS Appl. Eng. Mater.*, 2025, **3**(7), 2176–2189.
45 X. Yang, T. Shi, B. B. Gao, L. Li and S. D. Zhang, Ultralow-Smoke-Release Epoxy Resin with Efficient Radical Quenching Fabricated *via* Soluble Carbohydrates, *Ind. Eng. Chem. Res.*, 2024, **63**, 16789–16800.
46 B. B. Gao, T. Shi, X. Yang and S. D. Zhang, Online formation of epoxy resin multi-hierarchical char layer to improve mass and heat barrier performance *via* designable "heterogeneous char-forming agent", *Composites, Part B*, 2022, **246**, 110145.